Semiconductor Physics, Quantum Electronics & Optoelectronics, 2012. V. 15, N 3. P. 183-199.

PACS 07.57.Kp, 85.60.Gz

IR region challenges: Photon or thermal detectors? Outlook and means

F. Sizov
V. Lashkaryov Institute of Semiconductor Physics, NAS of Ukraine,
41, prospect Nauky, 03028 Kyiv, Ukraine; e-mail: sizov@isp.kiev.ua

Abstract. Infrared (IR) detectors play now an increasing role in different areas of human activity (e.g., security and military applications, tracking and targeting, environmental surveillance, fire and harvest control, communications, law enforcement, space surveillance of the Earth, medical diagnostics, etc.). Discussed in the paper are issues associated with the development and exploitation of up to date basic IR radiation detectors and arrays. Recent progress of basic for applications focal plane arrays (FPAs) that has rendered significant influence on infrared imaging is analyzed, and comparison of FPA detector performance characteristics is described with account of operational conditions and performance limits.

Keywords: IR detectors, FPAs, MCT and uncooled detectors.

Manuscript received 20.07.12; revised version received 27.08.12; accepted for publication 10.09.12; published online 25.09.12.

1. Introduction

Infrared detectors are applied for radiation detection and objects imaging when they emit radiation, having a temperature above 0 K. The nude human body ($T \sim$ 310 K) emits in all spectra from $\lambda = 0$ to $\lambda = \infty$ according the Stefan-Boltzmann law $W(T) = \sigma_B \cdot T^4$ about 1 kW into environment. Here $\sigma_B = 5.6686 \cdot 10^{-12}$ W/(cm$^2 \cdot$K^4) is the Stefan-Boltzmann constant and it is assumed that the surface area of human body is $S \approx 2$ m^2. At the same temperature of an environment the human body is in equilibrium with it and therefore does not lost energy. But e.g. at an environment temperature lower $\Delta T \approx 20$ K the human body one the heat losses are about 250 W and an undressed person will quickly chill. According to the Wien law, the wavelength max λ_{max} of emitted radiation intensity depends on temperature as $\lambda_{max} \cdot T =$ 0.2898 cm·grad.

Intuitively people has always been convinced that imaging in IR range is an extremely useful technology for getting an additional information of objects that are invisible (e.g. under night conditions) for human eye which is only sensitive within the spectral range approximately 0.4 to 0.75 μm.

IR detectors have started with William Herschel's experiments with thermometer in 1800. First, their development in 19th and early 20th centuries was mainly connected with thermal detectors, such as thermocouples and bolometers. The second kind of detectors, called photon detectors, was mainly developed during the 20th century. The photon effect based on photoconductivity was discovered by W. Smith in 1873, when he experimented with selenium as an insulator, but the first IR photoconductor detector was developed by T.W. Case in 1917 on the base of Tl_2S. In 1904, verily a photovoltaic detector in galena (natural PbS) – solid-state diode detector to detect EM waves – was patented by J. Bose ("Detector for electrical disturbances").

The period between World Wars I and II can be characterized as the development period of photon detectors and image converters. These were the image tubes (now called intensifiers with photocathode, micro-channel plates and fluorescent screen as the basic elements), which are sensitive in the shortest range ($\lambda \sim$ 0.8–1.2 μm) of IR spectra. The idea of an image tube was first proposed by G. Holst and H. De Boer in 1928. In 1934, Holst created the first successful IR converter tube (Holst' cup (glass)). This tube consisted of a photocathode in close proximity to a fluorescent screen. Electrons knocked out from the photocathode by IR photons were striking the fluorescent screen thus transferring an IR image into the visible region.

In 1933, E.W. Kutzscher (Germany) discovered that lead sulphide (PbS) is photoconductive to about

© 2012, V. Lashkaryov Institute of Semiconductor Physics, National Academy of Sciences of Ukraine

3-μm wavelength. These detectors were the first practical infrared detectors that have found a variety of applications during the World War II. After World War II, R.J. Cashman in USA found that other lead salts (PbSe and PbTe) can be used as infrared detectors. Since World War II, the IR detector technology development was primarily driven by military applications. In 1959, narrow band-gap mercury-cadmium-telluride (MCT) ($Hg_{1-x}Cd_xTe$, W.D. Lawson and co-workers) with variable ban-gap was shown to be applied for IR detectors with the sensitivity wavelength changeable by chemical composition "x". This opened a new era in IR detector technology.

The development of IR technology was dominating by photon detectors almost up to the end of 20th century. The essential drawback of photon detectors is the need of cryogenic cooling. This is necessary to prevent the charge carriers thermal generation.

The second revolution in thermal imaging began in the last decades of the 20th century after using the results of investigations of small area and mass of un-cooled thermal detectors for military and civilian applications. In the recent few years, development of un-cooled thermal detectors for thermal imaging resulted in many mainly commercial applications. Throughout the late 1970's and early 1990's, several companies developed un-cooled thermal devices based on various thermal detection principles, which were possible to assemble into arrays. They have started with ferroelectric barium strontium titanate ($BaSrTiO_3$) detectors (Texas Instruments, USA) and microbolometers (Honeywell, USA) and later with α-Si (LETI + ULIS, France). Among other countries developing their own cooled and uncooled FPA technologies for commercial and military applications are UK, Japan, South Korea, Canada, China, Italy, Russia, and others. Fig. 1 reflects the countries whose papers are drawn from Web of Science citation database. By comparing the number of publications that have emerged from various countries over the last 30 years, one can see acceleration in research reporting by most of the countries (after [1]).

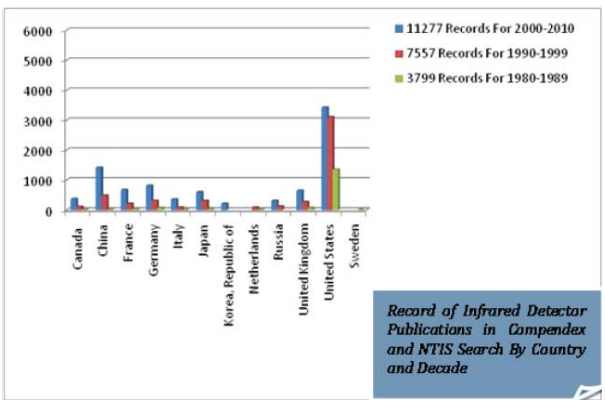

Fig. 1. Illustrative global infrared detection publication activities [1].

Now these technologies are well mastered by several companies: Raytheon, BAE Systems, DRS Technologies, FLIR, L–3 Communications, Sensors Unlimited – Goodrich and some others (USA), NEC, Mitsubishi (Japan), XenICs (Belgium), SCD (Israel), INO (Canada) and so on.

In comparison with photon detectors, thermal detectors were less exploited because to 1970s they were rather slow and had lower sensitivity in comparison with photon detectors. But making sensitive pixels small and thin, it is possible to decrease the response time considerably as the thermal constant time $\tau_{th} = C_{th}/G_{th}$ can be about $\tau_{th} \sim 20$ ms and less, where the thermal capacity $C_{th} \sim 2 \cdot 10^{-9}$ J/K for VO_x or α-Si:H microbolometers with typical dimensions ~50×50×0.5 μm and for them thermal-conductivity coefficient $G_{th} \sim 10^{-7}$ W/K.

Beginning from late 1970s, the progress in the number of detectors in the detector arrays, which revolutionized IR technologies and made them much more cost effective, was primarily connected with application of silicon readout circuits (ROICs). Assembling ROICs with different types of detectors allowed to build up the IR focal plane arrays (FPAs), which now can contain about 10^8 IR detectors. Applications of these technologies made possible discretization of process of image creation as well as its processing by the instrumentality of linear and matrix detector arrays from discrete elements.

The history of IR detectors in different periods and detector types is well presented in a number of papers and books (see e.g. [2–6]).

Here, in a short review, the attempt to compare the advantages and drawbacks of IR photon and thermal detectors and FPAs, mainly manufactured on the base of HgCdTe narrow-gap semiconductor and microbolometers, will be discussed, and comparison of nowadays arrays on the base of both these types of detectors will be presented. Mainly the state of the art and near-term developments of existing IR detector achievements will be pointed out.

Parameters of IR detectors and FPAs (e.g. their sensitivity, which can be characterized by noise equivalent power (NEP), detectivity (D^*) or noise equivalent temperature difference (NETD), dimensions of sensitive elements, and some others) are critical in the final analysis of objects detection, recognition and identification ranges.

Here, we will not consider the features of ROICs (read-out integrated circuits), though the IR FPA consist of an array of IR detectors, which absorbs photons and generate small voltage signals, and a ROIC connected to it (e.g. hybridized via In bumps) that amplifies and multiplex these voltages. It is only worth noting that many process technologies developed for 65, 45, or 32 nm, widespread and adjusted for digital circuit performance, are less than ideal for the analog processes

© 2012, V. Lashkaryov Institute of Semiconductor Physics, National Academy of Sciences of Ukraine

needed for a pixel and ROIC information processing. For IR megapixel array, huge ROICs are needed (see Fig. 2) which involve some kind of special technological processes. Testing procedures of large arrays, which require the huge data throughput circuits and high-speed computer capabilities, also will not be considered. These are the separate not simple tasks.

Narrowing the discussion here substantially to two types of IR FPAs (photon MCT and uncooled microbolometers) is conditions here as by limited sizes of paper and mainly by the fact of readiness of the current development of different types of technologies for FPAs production. Presented in Table 1 are technology readiness levels (TRLs) for different types of IR detector arrays. The highest level of TRL is 10.

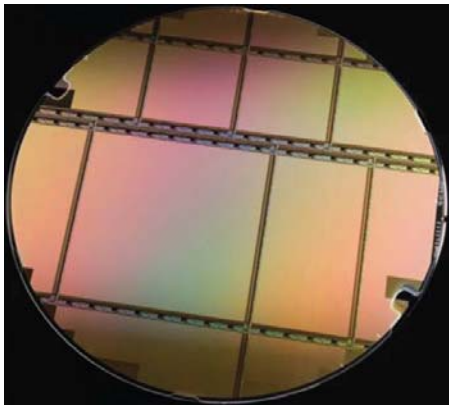

Fig. 2. 8-inch SB395 ROIC wafer from 2007 Raytheon industry research and development with 4K×4K, 2K×4K and 2K×2K die [7].

2. Classification of infrared detectors

In detectors, transformation of absorbed electromagnetic radiation ending, as a rule, as an appearance or changing of electrical signals takes place. This absorbed radiation heats electron or lattice (atom) subsystem leading to alterations of their properties, or changes electron energy distribution, thus modifying the motion of charged carriers. Such alterations are fixed by measuring the changes of detector physical parameters.

The majority of IR detectors can be classified into two main categories: photon detectors (also called quantum detectors) and thermal detectors. These two categories in turn can be subdivided into a large number of different kind detectors. E.g., mentioned among photon detectors can be the following devices: photodiodes, photoconductors, photoemission detectors, photo-MIS (MIS – metal-insulator-semiconductor) and photo-CCD

Table 1. Comparison of LWIR existing state-of-the-art device systems for LWIR detectors ([1]).

Maturity	Bolometer	HgCdTe	Type II SLs	QWIP	QDIP/QDWIP
	TRL 9	TRL 9	TRL 2-3	TRL 8	TRL 1-2
Status	Material of choice for application requiring medium to low performance	Material of choice for application requiring high performance	Research and development	Commercial	Research and Development
Military System Examples	Weapon sight, night vision goggles, missile seekers, small UAV sensors, unattended ground sensors	Missile intercept, tactical ground and airborne imaging, hyperspectral, missile seeker, missile tracking, space-based sensing	Being developed in universities and evaluated in industry research environment	Being evaluated for some military applications	Very early stages of development at universities
Limitations	Low sensitivity and long time constraints	Performance susceptible to manufacturing variations. Difficult to extend to >14 micron cut-off	Requires a significant, >$100 million, investment and fundamental material breakthrough to mature	Narrow bandwith and low sensitivity	Narrow bandwith and low sensitivity
Advantages	Low cost and requires no active cooling. Leverages standard Si manufacturing equipment	Near theoretical performance. Will remain material of choice for at least the next 10-15 years	Theoretically better then HgCdTe at >14 micron cut-off. Leverages commercial III-V fabrication techniques	Low-cost applications. Leverages commercial manufacturing processes. Very uniform material	Not sufficient data to characterize material advantages

*LWIR – long wave infrared (IR) (spectral region 8-14 μm), SL – superlattice, QWIP – quantum well IR photodetector, QDIP – quantum dot IR photodetector.

© 2012, V. Lashkaryov Institute of Semiconductor Physics, National Academy of Sciences of Ukraine

(CCD – charged-coupled-devices) detectors, intensifiers, photon-drag effect detectors, phototransistors, etc. Among thermal detectors one can note: pyroelectric (ferroelectric) detectors, thermometers, bolometers, bimetallic detectors, superconductive detectors, pneumatic (Golay cell) detectors, etc. It is difficult there to compare the advantages and drawbacks of all detectors. To be proper acquainted with IR detectors and FPAs, one can turn, e.g., to [6, 8]. Only some properties and characteristics of the most used in imaging and surveillance applications will be shortly considered.

In ***photon detectors***, which are mainly semiconductor detectors, radiation is absorbed directly by the radiation sensitive material – by electrons either bound to lattice atoms (being in the valence band – intrinsic detectors) or by impurity atoms (extrinsic or impurity detectors), or with free carriers (free carrier detectors) inside the valence or conduction bands and in metal near metal-semiconductor interface (photoemission detectors – Schottky barrier detectors (SBDs)) (see Fig. 3). Charge carriers generated in a photon detector by radiation absorption can be sensed directly (voltage or current), and the response of photon detectors is proportional to the number of absorbed photons.

These processes in photon detectors are not going with notable changes of sensitive element (e.g. detector lattice) temperature as compared to that of thermal detectors. Photon detectors respond only to photons, the energy of which exceeds some threshold values, e.g. semiconductor band-gap (intrinsic detectors), ionization energy of impurity levels in semiconductors (impurity or extrinsic detectors) and quantum levels in quantum wells (QWs), quantum dots (QDs), and superlattices (SLs) (QW, QD or SL detectors), SBD height ($q\varphi_b$), etc. (Fig. 3). This is a reason why photon detectors show a selective wavelength dependence of response (Fig. 4). To achieve good signal-to-noise ratio, the IR photon detectors for 3–5 and 8–14 μm regions (MWIR – medium wavelength IR and LWIR – long wavelength IR) as a rule require cryogenic cooling (down to $T \sim$ 80–150 K) to suppress the thermal generation of charge carriers. These detectors are fast (response time $\tau \sim 10^{-4} - 10^{-10}$ s) as compared to un-cooled thermal detectors (response time $\tau \sim 10^{-1} - 10^{-2}$ s).

The longwave limits to photon detectors, when now exist narrow-gap solid solutions with variable band-gaps (e.g. $Hg_{1-x}Cd_xTe$) or impurities with small excitation energies (Ge:x, Si:x), or QWs and SLs with shallow quantum levels, depend mainly on available operation temperatures. For a photon detector to be effective, the generation rate g of carriers excited by radiation should be considerably higher than the thermo-generation rate g_{th}

$$g = \eta\alpha N_{ph} >> g_{th} = n_{th}/\tau. \quad (1)$$

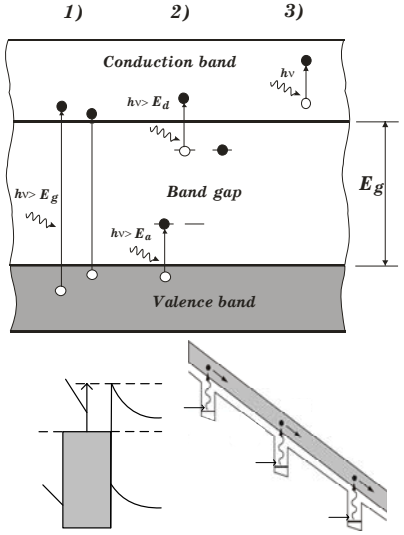

Fig. 3. Photon mechanisms of electron subsystem excitation in photon detectors: 1) intrinsic excitation, 2) impurities excitation, 3) free-carriers absorption, 4) absorption in SBD, 5) absorption in QWs (SLs).

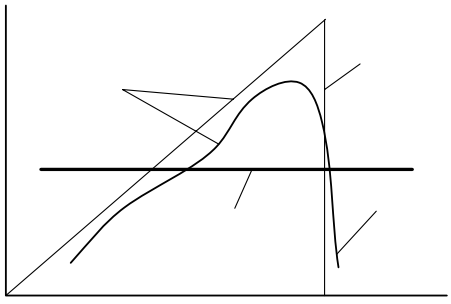

Fig. 4. Relative spectral response dependences of photon and thermal detectors.

Here, α is the radiation absorption coefficient, η – quantum efficiency, N_{ph} – number of photons falling down onto detector, n_{th} – number of thermo-generated carriers, and τ – their recombination time. For a typical quantum (photon) IR detector (e.g., narrow-gap HgCdTe or extrinsic Ge ($\alpha \sim 10^3 - 10^2\,\text{cm}^{-1}$, $\eta \sim$ 0.5–0.2)) and $N_{ph} \sim 6\cdot10^{13}\,\text{cm}^{-2}\text{s}^{-1}$ (at $\lambda \sim$ 300 μm, $\Delta\lambda \sim$ 40 μm for black-body radiation at $T =$ 300 K, field of view FOV = π sr) $g = \alpha\eta N_{ph} \sim (0.1-3)\cdot10^{16}\,\text{cm}^{-3}\text{s}^{-1}$. For Ge (or HgCdTe with $E_g \approx$ 4 meV at $T \sim$ 4 K), the thermo-generation rate from impurities or intrinsic carrier concentration (for HgCdTe $n_{th} \sim (10^{12} - 2\cdot10^{11})\,\text{cm}^{-3}$), and typical $\tau \sim (10^{-7} - 10^{-10})\,\text{s}^{-1}$, $g_{th} \sim (2\cdot10^{18} - 10^{22})\,\text{cm}^{-3}\text{s}^{-1} >> g$. For spectral range of $\lambda \sim$ 45 μm, $\Delta\lambda \sim$ 10 μm, $N_{ph} \sim 2.5\cdot10^{17}\,\text{cm}^{-2}\text{s}^{-1}$ for the same

© 2012, V. Lashkaryov Institute of Semiconductor Physics, National Academy of Sciences of Ukraine

FOV and for HgCdTe (band-gap $E_g \sim 0.025$ eV at $T = 80$ K) $n_{th} \sim 3.5 \cdot 10^{15}$ cm^{-3}. Thereby $g_{th} >> g$, too.

Similar relations are valid for extrinsic and QW (SL) detectors. This kind of detectors will be inefficient in far IR spectral region ($\lambda > \sim 50$ μm) with their operation temperature $T > 30$ K, as it is well known, e.g., for impurity detectors [9], SL and intrinsic (e.g., HgCdTe) detectors [6]. Operation of photon far IR detectors is questionable in this temperature range (one exception is PbSnTe:In photoconductor, in which τ is extremely long [10] at $T < 20$ K).

It is interesting to note that for photon detectors operating in back-ground limited performance (BLIP) regime when their characteristics are limited only by back-ground photon flux fluctuations (and now almost all IR intrinsic photon detectors for 3–5 and 8–12 μm spectral ranges operate in BLIP regime) the most preferable spectral range (in Earth environmental conditions with temperature of background $T_b \approx 300$ K) for passive vision is the spectral range $\lambda \approx 8$–28 μm [8]. Shift of the detector cut-off wavelength into the far IR region do not result in sufficient increase, e.g., of Earth surface thermal contrasts.

Among a long array of materials proposed for photon detectors the fundamental properties of $Hg_{1-x}Cd_xTe$ narrow-gap semiconductors (high optical absorption coefficient, high electron mobility and low thermal generation rate), together with the capability for band-gap energy engineering changing the chemical composition *x*, make these alloy systems almost ideal for a wide range of IR detector applications. One of the problems is growing HgCdTe material, significantly due to the high vapor pressure of Hg. But to the date, this problem is partially overcome by growing the epitaxial layers with different kinds of techniques (e.g., liquid phase epitaxy or molecular beam epitaxy) under controllable conditions.

The possibility of band-gap mercury-cadmium-telluride (MCT) energy engineering resulted in different IR detector application ranges: from short wavelength IR (SWIR: 1–3 μm) to middle wavelength IR (MWIR: 3–5 μm), long wavelength IR (LWIR: 8–14 μm), and very long wavelength (VLWIR: 14–30 μm). HgCdTe technology development was and continues to be dominating for military applications where high sensitivity, fast frame operation, diffraction limited pixel sizes and high fill factors are of primary needs. The BLIP current for LWIR HgCdTe applications, looking at a $T_b = 300$ K with *F*/1 optics at $T_d = 77$ K and $\lambda_{co} \sim 12$ μm, is much higher (~ 0.18 A/cm^2) as compared to the dark current of photodiode ($\sim 10^{-4}$ A/cm^2) allowing operation of HgCdTe FPAs in the BLIP regime [1].

In ***thermal detectors,*** the absorbed radiation is transduced, as a rule, into a change of their electrical parameters. For microbolometers, e.g., the registration process of the incident radiation can be realized by three different parts of such detectors. They are, as it seen for example in Fig. 5, an IR absorber, a thermal isolation layer, and a temperature sensor. The incident radiation is absorbed in IR absorber in which IR electromagnetic energy is converted into heat energy of a thermally isolated sensor thus changing its physical properties (e.g., resistivity, dielectric permittivity, thermo-electric effect, thermo-mechanical effect) that lead to changes in a measurable output parameters.

Relative spectral response of these detectors, because of the absence of threshold barriers in process of radiation absorption, should not depend on the wavelength (Fig. 4), though some wavelength dependence response can occur due to design peculiarities of thermal detectors and, e.g., emissivity factor spectral dependence changes of coating layers used to increase the radiation efficiency coupling with thermal sensitive elements. Typical single-level bolometer design is shown in Fig. 6. The typical values of temperature coefficient changes for VO_x and α-Si microbolometers are within $\alpha_{th} \sim 0.02 - 0.05$ K^{-1}.

Different types of uncooled detectors are available now on the market. They are made of different and frequently unconventional materials with their own benefits but really now only three types of such detectors are widespread in infrared technologies [6, 12]. They are VO_x, α-Si microbolometers, and ferroelectrics (group of pyroelectric materials) detectors based, e.g., on barium strontium titanate (BST) which allow detectors assembling into large arrays with ROICs. Shown in Fig. 7 is an estimated market shares for VO_x, α-Si and BST detectors.

Developing both VO_x microbolometers and BST detectors in 1980s at USA, it was believed that in thermal imaging systems with uncooled detectors military would have a choice of technology [12]. But about 10 years ago the situation has changed. At that time, convinced of the advantages VO_x over BST, the US Military decided not to provide any more funding for research into BST technology. From that point in time, only further research in VO_x was supported [12]. Moreover, because of the need of thin small area thermal detectors in large arrays, certain difficulties arise, as most ferroelectrics tend to lose their properties as the thickness is reduced and there exist difficulties in manufacturing diffraction limited pixels.

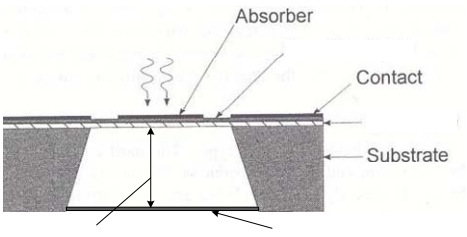

Fig. 5. Schematic of microbolometer constituent parts.

© 2012, V. Lashkaryov Institute of Semiconductor Physics, National Academy of Sciences of Ukraine

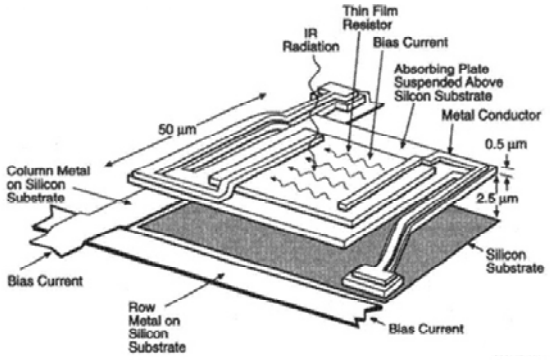

Fig. 6. Typical single-level bolometer design [11].

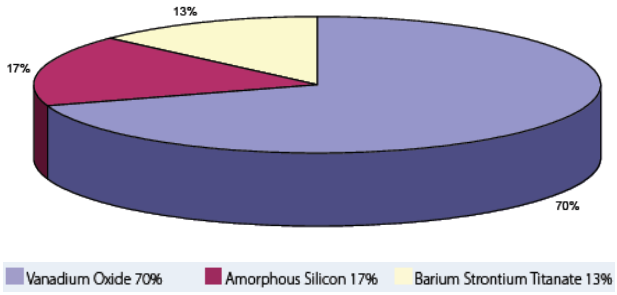

Fig. 7. Estimated market shares for VO_x, a-Si and BST detectors [12].

Thin film resistive microbolometers were first considered in early 1980's [13, 14]. Uncooled infrared microbolometers and focal plane array technology developed at Honeywell and which since that time has been widespread rapidly was published since the late 1980's [15]. (For full list of Refs. on the subject see e.g. [6, 16].)

A number of books, book chapters and review articles concerning infrared physics and different infrared technologies, including uncooled infrared detectors operation principles, have been published in recent years (for Refs. see [6, 8, 11, 17, 18]).

More than 10 years ago the system application roadmap for uncooled arrays was considered [19] (see Fig. 8). As the performance improves and pixel density increases, the number of military applications increases significantly. For the $2{\cdot}10^5$ 100 mK NETD pixels, simple surveillance and night driving enhancers were thought to be good applications. As the pixel density increased (with pitch decreased up to 10-20 μm as for cooled arrays, see [20]) and $\geq 10^6$ pixels became feasible, lightweight helmet sights, munitions, rifle sights, and unattended ground sensors became feasible, too. If the goals of the DARPA program comes to fruition (10 mK NETD), then advanced threat warning, long range scouts, and unmanned air vehicle applications can be realized.

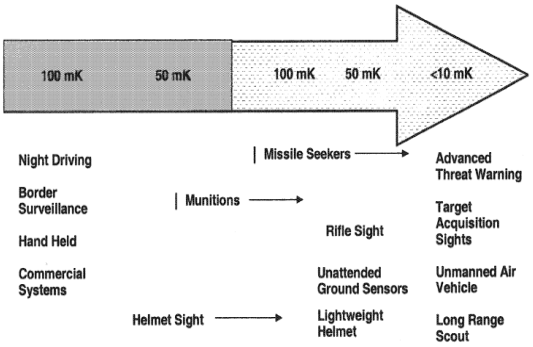

Fig. 8. System application roadmap uncooled IR FPAs [19].

3. Ultimate performance. Theoretical background. Information capacity

Vision is the most important of human senses, as more than 80% of information of an environment people are getting by vision. But spectral range in which a human eye is sensitive to radiation is very narrow though the number of photons that mainly defines the information capacity is high because of coincidence of eye max sensitivity and the Sun max radiating emissivity. Shown in Fig. 9 are the spectral dependences of Sun and Earth spectral radiances, and also Earth atmosphere transparency. Shown are the spectral radiance and not spectral radiant exitance dependences, as usually. It is made in order to present smaller difference between these curves.

The very important fact for efficiency of human vision is that the Earth atmosphere is transparent (without fog or rain) in visible spectral range. As one can see, it is also rather transparent in 3–5 and 8–12 μm IR spectral ranges, which makes the technical vision systems informative in these spectral ranges. And this is one of the reasons why the IR technical vision systems are the most widespread systems in these spectral bands. The second reason is the radiation intensity of objects at $T \sim$ 300 K (e.g., the mean temperature of the Earth surface heated by Sun radiation is $T \approx 293$ K) has max at $\lambda \approx 9.7$ μm.

Information capacity. Today, IR technologies are finding use in imaging, information and telecommunication technologies. Every photon bears information. For the case of only the noise connected with photon flux fluctuations dispersion $\langle \Delta N_{\text{ph}} \rangle \sim \langle (N_{\text{ph}}) \rangle^{1/2}$ (Poisson statistics ($h\nu >> k_{\text{B}}T$), where N_{ph} is photon number in the photon's flux), the system information capacity C_M (with M sensitive elements in array or M-number of decomposition elements in the image) is defined by [22]

$$C_M = \frac{M}{8} \log_2 \left[\frac{1}{k} \sin\left(\frac{\theta}{2}\right) \sqrt{\eta A_d \tau_{\text{acc}} N_{\text{ph}}} \right], \text{ byte.} \quad (2)$$

© 2012, V. Lashkaryov Institute of Semiconductor Physics, National Academy of Sciences of Ukraine

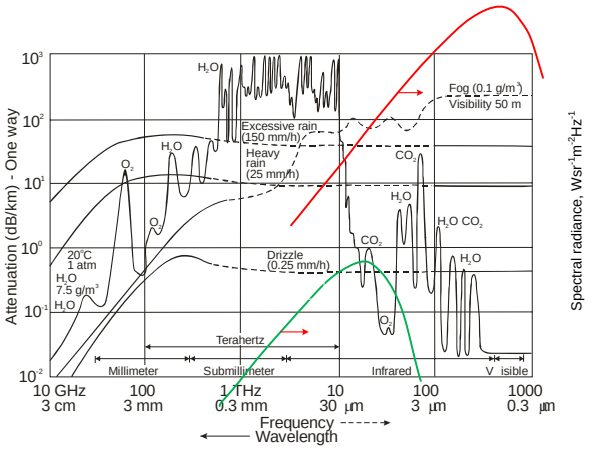

Fig. 9. Earth atmosphere transparency from visible to radiofrequency band regions (after Ref. [21]). Also are shown spectral radiances of blackbodies with temperature $T \approx 6000$ K (Sun) and $T \approx 300$ K (Earth).

This expression defines the upper limit information capacity of a vision system in one spectral region in the case of only the noise connected with the photon flux fluctuations. Here, k is the signal-to-noise threshold ratio, A_d – detector area, η – detector quantum (coupling) efficiency, τ_{acc} – accumulation time, N_{ph} – number of photons falling down on the detector, and θ – plane angle of view. It should be $k > 2$, as at $k = U_{thr} \Big/ \sqrt{\langle U^2_{noise} \rangle} = 1$ the probability of false signal is equal $P_{fs} = 0.159$, i.e., it is a relatively large quantity. At $k = U_{thr} \Big/ \sqrt{\langle U^2_{noise} \rangle} = 2$ the probability of false signal is only 0.023 and is rapidly decreasing with k increase.

It is seen that the number of detectors or number of decomposition elements in the image M is a key parameter that determines the information capabilities of the system, as the other parameters are under the logarithm. At the same time, the accumulation time τ_{acc} (or "dwell" time τ_d) at each sensitive element is proportional to the number M_e of sensitive elements in the array and inversely proportional to the frame rate f_r and number of picture dots M: $\tau_{acc} = 1/f_r \cdot (M_e/M)$. It is interesting to note that detector quantum efficiency plays not very important role, as it is under the square root and logarithm. This is a reason why the low quantum efficiency Schottky barrier diode (SBD) and quantum well (QW) or superlattice (SL) arrays are efficient in staring vision applications.

Advances in IR sensor technologies have enabled increasing the array sizes and decreasing the pixel sizes to get megapixel arrays [1, 23]. Fig. 10 shows the timeline for HgCdTe FPA development at Raytheon Vision Systems (RVS, formerly Santa Barbara Research Center, SBRC). High requirements exist for homogeneity properties and flatness of detector materials and silicon wafers for ROICs. E.g., a single 4K×4K ROIC die is longer than 8 cm along its side. The flatness requirements are equivalent to having a circular lake one mile in diameter with no ripples across the entire lake higher than three inches. Dealing with this type of flatness over huge thermal ranges requires in-depth understanding of all the thermal expansion properties of the materials used [7].

In spite of much larger photon fluxes appearing from the environment or thermal sources in IR regions because of growing an effective areas of detectors that are increasing up according to a diffraction limit $A_d \sim A_{dif} \approx 2.44 \cdot \lambda \cdot F/\#$ and also broad spectral range $\Delta\lambda \approx 8$–14 μm, the information capacity per one sensitive element in visible and IR ranges are comparable ($C_{vis} \approx 1.8$ bytes, $C_{IR}(8–14\ \mu m) \approx 1.9$ bytes [8]). This is because the contrast coefficient in IR region is much less. Here, F/# is the f-number of the optical system.

Important figures of merit for infrared detectors and system performances are the current or voltage or sensitivity $S_{I,V}$, the detectivity D^*, the noise equivalent power NEP and the noise equivalent temperature difference NETD (or, which is the same, NEDT) [6, 24]. Sensitivity measures the electrical signal output $[I_s(V_s)]$ per radiation incident power $S_{I,V} = I_s(V_s)/W$. D^* and NEP are joined with each other by the equation $D^* = (A_d \cdot \Delta f)^{1/2}/\text{NEP}$, where A_d is the detector active area and Δf is the system bandwidth. NEP $= W \cdot (I_s/I_n) = W \cdot (V_s/V_n)$, where $I_n(V_n)$ is the noise signal.

NETD is one of the most important performance parameters for infrared imaging systems and is defined as the change in the extended equivalent blackbody temperature that corresponds to a change in radiance, which will produce a signal-to-noise ratio $I_s/I_n = 1$ or $V_s/V_n = 1$ in an infrared detector or system.

The classical expression for NETD in the case of only background fluctuations can be written as in [24]

$$\text{NETD} = \Delta T = \frac{4(\text{F}/\#)^2 \cdot (\Delta f)^{1/2}}{A_d^{1/2} \cdot \int_{\lambda_u}^{\lambda_{co}} \frac{\partial W(\lambda, T)}{\partial T} \cdot \tau_{op} \cdot \tau_{atm} \cdot \tau_f \cdot D^*(\lambda, T) \cdot d\lambda}, \text{ K}, \quad (3)$$

T≈300 K

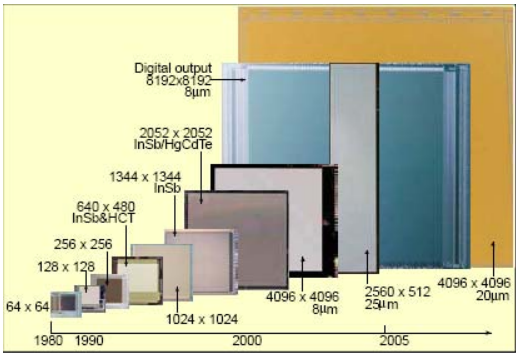

Fig. 10. Prorgression of ROIC format at RVS over time [7].

© 2012, V. Lashkaryov Institute of Semiconductor Physics, National Academy of Sciences of Ukraine

where τ_f, τ_{op} and τ_{atm} are the transmission coefficients of optical filter (as a rule cooled), optics and atmosphere, respectively, A_d is the detector active sensitive area, Δf – bandwidth, λ_{co} – detector cut-off wavelength and λ_u – filter short part of the wavelength transparency waveband.

The NETD includes contribution of NETD different parts and can be expressed by the common expression written, e.g., for bolometers [25], but it can be applied to any kind of detector array adding terms with additional noise

$$\begin{aligned}\mathrm{NETD}^2 &= \mathrm{NETD}^2_{1/f} + \mathrm{NETD}^2_{\mathrm{J-N}} + \\ &+ \mathrm{NETD}^2_{\mathrm{thermal}} + \mathrm{NETD}^2_{\mathrm{ROIC}},\end{aligned} \tag{4}$$

where the total NETD consists of the $\mathrm{NETD}_{1/f}$ from the $1/f$-noise, the $\mathrm{NETD}_{\mathrm{J-N}}$ from the Johnson-Nyquist noise of the detectors, respectively, the $\mathrm{NETD}_{\mathrm{thermal}}$ from the thermal fluctuation noise of the detectors including background fluctuation noise, and the $\mathrm{NETD}_{\mathrm{ROIC}}$ from the read-out integrated circuit (ROIC) related noise. Not all the noises are included in this expression. There also can be important fixed pattern noise, temporal noise, etc.

3.1. Photon detectors. Upper limit performance

The upper limit performance of up-to-date IR photon detectors in 3–5 and 8–14 μm spectral bands at $T \sim$ 300 K environment conditions is mainly restricted by fluctuations of photon fluxes (background limited performance – BLIP regime). NEP value that characterizes the detector sensitivity in the case of ideal photodiode detectors can be written for the given wavelength λ (Poisson statistics, $T \geq 300$ K, $\lambda \leq 25$ μm) as [6, 8, 24])

$$\begin{aligned}\mathrm{NEP} = \frac{I_n}{S_I} = \frac{\left\langle I_n^2 \right\rangle^{1/2}}{S_I} = h\nu \cdot \sqrt{\frac{2 \cdot N_{\lambda,T}}{\eta}} \cdot \sqrt{A_d \cdot \Delta f} = \\ = \sqrt{\frac{2 \cdot h\nu}{\eta} \cdot W_{\lambda,T}} \cdot \sqrt{A_d \cdot \Delta f},\end{aligned} \tag{5}$$

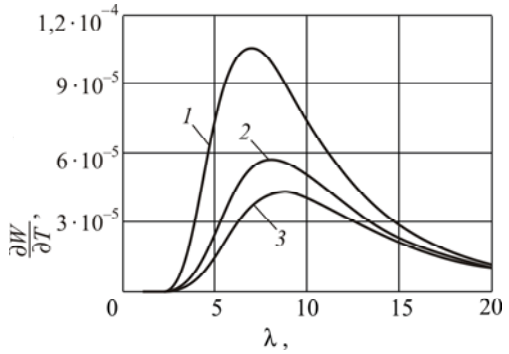

Fig. 11. Dependence of derivative $\partial W/\partial T$ of Planck' law on wavelength for different temperatures. T, K: *1* – 320, *2* – 300, *3* – 280 [8].

where I_n is the detector noise current, S_I – detector current sensitivity, $N_{\lambda,T}$ and $W_{\lambda,T}$ are the number of photons and radiation power density at the wavelength λ and temperature T, η is the detector quantum efficiency, A_d – detector area, and Δf – bandwidth.

In the spectral range ($\Delta\lambda = \lambda_u - \lambda_{co}$), the number of photons and radiation power density (from black body) are defined by the Planck radiation law

$$N_{T,\lambda} = \frac{\Omega_i}{\pi} \cdot \int_{\lambda_u}^{\lambda_{co}} \frac{2\pi c}{\lambda^4 \left[\exp\left(\frac{hc}{k_B T \lambda} \right) - 1 \right]} \cdot d\lambda,$$

$$W_{T,\lambda} = \frac{\Omega_i}{\pi} \cdot \int_{\lambda_u}^{\lambda_{co}} \frac{2\pi hc^2}{\lambda^5 \left[\exp\left(\frac{hc}{k_B T \lambda} \right) - 1 \right]} \cdot d\lambda, \tag{6}$$

where $\Omega_i = \pi \cdot \sin^2(\theta_i/2)$ is the detector FOV and θ – detector plane angle of view.

To make NETD smaller, the components in (3), namely, D^* and $\partial W/\partial T$, should have maximum values. The function $\partial W/\partial T$ maximum at the object temperature $T =$ 300 K is at $\lambda =$ 8.035 μm, and it is smoothly declining with wavelength increase and is much more steep going to 3–5 μm region (see Fig. 11).

For photon detectors with different cut-off lengths, the detectivity $D^*_\lambda(\lambda)$ is increasing with wavelength decrease to a great degree compensating the $\frac{\partial W(\lambda, T)}{\partial T}$-decline in a shorter, as compared to $\lambda \approx 8$ μm, wavelength band. This situation differs photon detectors from thermal ones in which $D^*_\lambda(\lambda) = D^* \approx$ const, and thus the systems with photon detectors operating in $\lambda <$ 8 μm spectral bands will have principally better parameters as compared to the systems with thermal FPAs.

As concerning the $D^*_\lambda(\lambda)$ values, most of IR photon detectors now are operating in the regime close to the BLIP one. For example, for HgCdTe detectors the detectivities reach $D^*_\lambda \approx 2 \cdot 10^{11}$ cm·Hz$^{1/2}$/W for $\lambda_{max} \approx$ 10.5–11 μm and FOV ≈ 30° ($\lambda_u \approx$ 7.8 μm, $\lambda_{co} \approx$ 11.2 μm, photon fluxes $N_{ph} \approx 3.3 \cdot 10^{16}\,\mathrm{ph \cdot cm^{-2} s^{-1}}$) for arrays with time delay and integration (TDI) function over 4 sensitive elements (see [26]), which gives the possibility to obtain NETD ≈ 9 mK. TDI function allows to increase the sensitivity approximately as square root of the number of elements.

High detectivity values for MCT arrays were obtained in [27] for the short IR range $\lambda_{co} =$ 1.8 μm when operating at 295 K, $D^*_\lambda \approx 1.4 \cdot 10^{12}$ cm·Hz$^{1/2}$/W. For relatively low background fluxes ($N_{ph} \approx 7.82 \cdot 10^{15}\,\mathrm{ph \cdot cm^{-2} s^{-1}}$) for 256×256 MCT array with $\lambda_{co} =$ 10.5 μm operating at $T =$ 85 K, the measured detectivity value was $D^*_\lambda = 3.9 \cdot 10^{11}$ cm·Hz$^{1/2}$/W, and for arrays with $\lambda_{co} =$ 15.8 μm operating at 40 K $D^*_\lambda = 2.76 \cdot 10^{11}$ cm·Hz$^{1/2}$/W [27]. For ideal, uncooled thermal detector $D^* = 1.813 \cdot 10^{10}$ cm·Hz$^{1/2}$/W at $T_b =$ 300 K.

© 2012, V. Lashkaryov Institute of Semiconductor Physics, National Academy of Sciences of Ukraine

Under assumption in (3) of F/# = F/1, $\tau_{op} \sim 1$, A_d = 30×30 μm, quantum efficiency $\eta = 0.65$ and $D^*_\lambda(\lambda, T) \approx 6 \cdot 10^{10}$ cm·Hz$^{1/2}$/W at $\lambda_{max} \approx$ 11–12 μm, which is typical for HgCdTe photodiodes at FOV ≈ 90°, the value of NETD ≈ 17 mK for the spectral range 8–12 μm, background temperature T_b = 300 K and rather wide bandwidth $\Delta f = 1/(2\tau_{acc}) \approx 25$ kHz that is unattainable for thermal FPAs (typical accumulation times for charge storage capacities of ROICs $\tau_{acc} \approx 20$ μs). At less wide spectral sensitivity band and larger accumulation times, the values of NETD will be lower (see Fig. 12).

The estimated value is very close for the NETD parameter attained now for photon detector arrays (see Table 2 below). For the wavelength band λ = 4.08–7.73 μm, much lower (because of high D^*_λ values) NETD values were received (NETD = 2.75 mK for 256×256 HgCdTe array at T = 95 K [29]).

By estimations of NETD for matrix arrays, the accumulation time τ_{acc} is practically equal to the frame time τ_{fr} on the assumption of no restrictions to accumulation time of ROICs charge handling capacities. Than at typical $\tau_{fr} \sim$ 50 Hz the accumulation time $\tau_{acc} \sim 2 \cdot 10^{-2}$ s and the bandwidth $\Delta f \approx$ 25 Hz, which is 10^3 times lower as compared, e.g., to detectors in linear arrays. Respectively, NETD would be square root times lower (see Exp. (3)).

In reality, charge storage capacities of ROICs are restricted as a rule by $C \sim$ 2–3 pC, because of the lack of sufficient area in silicon ROICs and, for spectral range 8–12 μm, because of high background fluxes $\tau_{acc} \sim$ 10–60 μs.

But small accumulation times of photon detectors give the possibility to increase the frame rate of IR systems. This is the difference of systems with arrays based on photon detectors, as compared to the systems based on uncooled thermal matrix arrays, in which the response times of each detector are much longer and these times control the frame rate of these systems.

To increase τ_{acc} of photon detector, one can decrease its λ_{co} to lower the photon flux noise. E.g., for HgCdTe in the spectral range 7.7–9.5 μm the accumulation time can be increased up to 400 μs (Fig. 12). At higher accumulation times, NETD of such arrays is restricted by charge storage capacities.

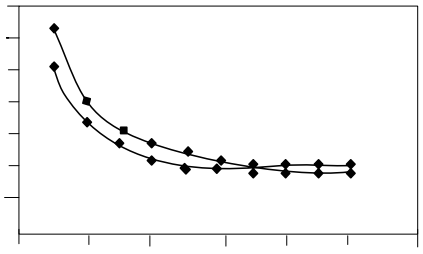

Fig.12. NETD as a function of λ_{co} and τ_{acc} for HgCdTe 320×256 matrix array [28]. λ_1 = 7.7 μm. A_d = (20×20) μm^2, F/# = 2.

In FPA with ROICs, the upper limit performance of the arrays with photon detectors is defined by the ROIC charge storage capacity value. The expression for NEDT can be written as [8, 30]

$$\mathrm{NETD} = 2\mathrm{F/\#} \cdot \frac{1}{\eta_{\mathrm{cold}}^2 (N_e)^{1/2}} \times \frac{\sqrt{\int_{\lambda_1}^{\lambda_2} N(\lambda) \cdot K(\lambda) \cdot \tau_f(\lambda) \cdot d\lambda}}{\int_{\lambda_1}^{\lambda_2} \tau_{\mathrm{op}} \cdot \tau_{\mathrm{atm}} \cdot \tau_f \cdot \frac{\partial N(\lambda, \dot{O})}{\partial T} \cdot d\lambda} \cdot \left(1 + \frac{\Delta N_n^2}{N_e}\right), \quad (7)$$

where $N(\lambda,T)$ is the photon number, ΔN_n – read-out noise of one sensitive element, N_e – number of electrons in charge storage capacity and η_{cold}^2 – efficiency of the cold diaphragm.

Shown in Fig. 13 are dependences of NEDT on the charge handling capacity N_e for different spectral bands inherent to MCT diode arrays with silicon ROICs [31]. One can see that NETD ~3 mK for MCT arrays cooled down to T = 78 K can be practically achieved and corresponds to a theoretical background performance limited only by the charge storage capacity of ROICs.

From (7), it particularly follows that in the case of functionality limitation by charge storage capacity, the NETD value does not depend on τ_{acc}, as one can see from Fig. 12.

The estimations of upper limit performance of photon detectors in BLIP regime show that for IR staring imager operating with the frame time $\tau_f \approx \tau_{acc}$ (τ_{acc} = 40 ms as about for thermal detectors), F/# = 1, and with the detector active area A_d = 30×30 μm and for $\lambda_{co} = \lambda_{min}$ = 28 μm $\mathrm{NEDT}_{min} \approx$ 0.17 mK (Fig. 14). For λ ~ 10 μm region, this value is ~12% worth, and thus the staring systems based on these detectors can be efficient ones for detection of small thermal contrasts [32].

For the 3–5 μm spectral region, the NETD is several times worth but still is low to be applicable for a lot of special and civilian purposes. The pixel number in FPAs is getting now $N > 10^6$ that is very important for long distance spatial resolution and identification of objects, and efforts of FPAs designers are directed to increase the number of pixels in arrays. As for example, shown in Fig. 15 are the measured and predicted the InSb FPA format and pixel density. Some examples of megapixel FPAs are also presented in Table 2.

The overall tendency in any imaging system is shrinking the pixel area. Small pixels in arrays allow implementation of high-resolution FPAs. At the same time, the important reason is the cost for both the FPA chip, and for the infrared optics it is reduced by shortening the active area of the FPA. Oversampling the diffractive spot may provide some additional resolution for smaller pixels. Shown in Fig. 16 is the tendency of shrinking the pixel in HgCdTe arrays.

© 2012, V. Lashkaryov Institute of Semiconductor Physics, National Academy of Sciences of Ukraine

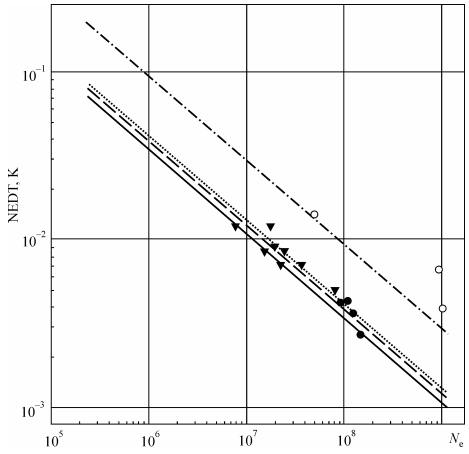

Fig. 13. Dependences of NEDT of MCT arrays at T = 78 K on charge handling capacity N_e for different spectral bands [31]. Upper curve and experimental points are for 7.8-10 μm band and bottom curves are different parts of 3-5 μm band.

Some parameters of several manufactures of HgCdTe, QW and InSb IR photon FPAs are presented in Table 2. They are typical for other cooled FPA producers and are taken from [6, 8] and some companies data sheets. Some nowadays HgCdTe cooled arrays allow fast sub-frame operations up to several thousand Hz. Parameters of InSb IR arrays for 3–5 μm region of other producers are similar to those presented in Table 2 for this spectral range. Advantages of HgCdTe, as compared to InSb, typically include higher temperature operation, as well as the critical inherent tunable spectral response of HgCdTe, which can readily be adjusted during semiconductor growth for short, middle, or long wavelength IR response [23].

The parameters of FPAs presented in Table 2 are for hybrid-packaged devices. This technology allows realization of near 100% fill factors and increased signal-processing area in the as a rule silicon ROICs. In hybrid technology, one can optimize the detector

Table 2. IR photon FPAs parameters of some major Manufactures.

Manufacturer	Array size	Pixel size or pitch, μm	NETD, mK	Spectral band, μm	Full frame rate f, Hz
DRS Infrared Technologies (USA)	256×256	40	8 (77 K), MCT	3-5	120
	640×480	25	10 (77 K), MCT	3-5	60
	640×480	25	13 (77 K), MCT	8-10.5	<60
	640×480	12	25 (F/3.25), MCT	3.4-4.8	30-120
	1024×768	16	15 (<140 K), MCT	3-5	
	640×512	24	12 (<140 K), MCT	3-5	
	640×512	24	13.5/26.6 (80 K), MCT	(3-5)/(8-10)	
FLIR (USA)	640×512	15	18 (F/2.5, 77 K), MCT	3.7-4.8	120, 3.0 kHz –windowing
	640×512	16	<30 (F/2, 77 K), MCT	7.85-9.5	115, 62 kHz min window
	640×512	15	<20 (F/2.5, 77 K), InSb	1.5-5.1	100, 1.8 kHz – min window
SOFRADIR (France)	1280×1024	15	18 (77-110 K), MCT	3.7-4.8	Up to120
	1000×256	30	(<200 K), MCT	0.8-2.5	Up to 250
	640×512	15	17 (F/2, <100 K), MCT	7.7-9.5	Up to 210
	640×512	15	<18 (F/2, <120 K), MCT	3.7-4.8	Up to 120
	384×288	25	17 (77-80 K), MCT	7.7-9.5	Up to 300
	320×256	30	20 (F/2, 70-90 K), MCT	7.7-11	Up to 200
	640×512	20	31 (70-73 K), QWIP	λ_p=8.5, $\Delta\lambda$=1	
AIM (Germany)	384×288	24	15/25, MCT	3-5/8-9	120
	640×512	24	<15 (F/1.5, 77 K), MCT	3-5	<200
	640×512	15	25/40	(3-5)/(8-9)	<100
	384×288×2	40	35/25, SL (QWIP)	λ_p=3.4.8/5.0	<100
Raytheon (USA)	640×480*	20	25 (F/5), MCT	(3-5)/(8-10)	70
	1024×1024	27	35 (80 K), InSb	0.6-5.0	13
	2048×2048	20	(70-80 K), MCT	0.85-2.5	
	2048×2048	15	23 (78 K), MCT	3-5	
	2048×2048	25	(30 K), InSb	0.6-5.4	
Teledyne Imaging Sensors (USA)	2048×2048	18	(140 K), MCT	1.65-1.85	
	2048×2048	18	(77 K), MCT	2.45-2.65	
	4096×4096	10 or 15	(77 K), MCT	1-2.5	
SCD (Israel)	1280×1024	15	20 (77 K), InSb	3-5	
JPL (USA)	256×256	38	40 (70 K), QWIP	λ_p~8.5	
	640×486	18	36 (70 K), QWIP	λ_p~8.5	
	1024×1024		(70 K), QWIP	(4-5)/(7.5-9)	30
BAE Systems (USA)	640×480	25	30/34 (F/2, 60 K), QWIP	λ_p=5.1/8.5	50

*QWIP – quantum well IR photodetector.

© 2012, V. Lashkaryov Institute of Semiconductor Physics, National Academy of Sciences of Ukraine

material and ROIC parameters independently, and then connecting the detector array and the ROIC, e.g. by In-bump technology.

Another important positive feature of hybrid technology is the possibility to shrink the pixel sizes preserving the NETD parameter. Pixel sizes up to 10-15 μm have been demonstrated in hybrid systems (see Table 2). Pixel reduction is required for lowering the cost of a system (weight and dimension decrease due to the optics diameter decrease, the cooling machine and cryostat size decrease, the power consumption reduction and the reliability increase).

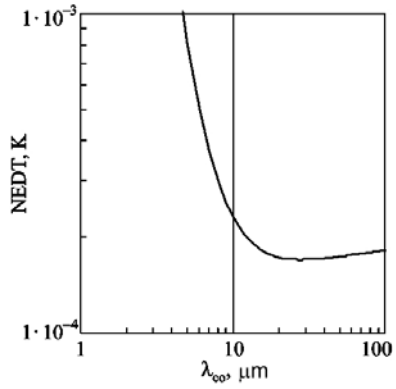

Fig. 14. Dependence of NEDT of ideal photodiode on λ_{co}. T_b = 300 K, τ_{acc} = 40 ms, F/# = 1, η, η^2_{cold} =1, A_d = 30×30 μm^2 [8].

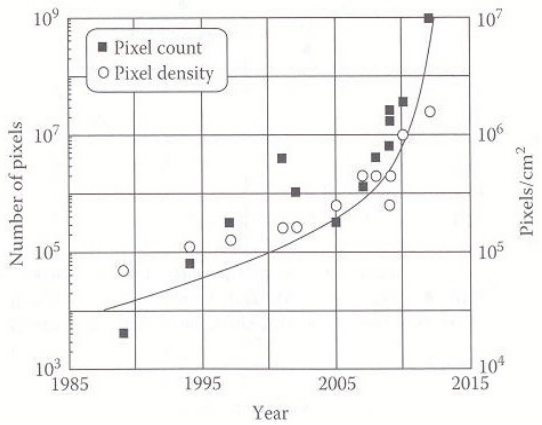

Fig. 15. Measured and predicted InSb FPA format and pixel density [6, 33].

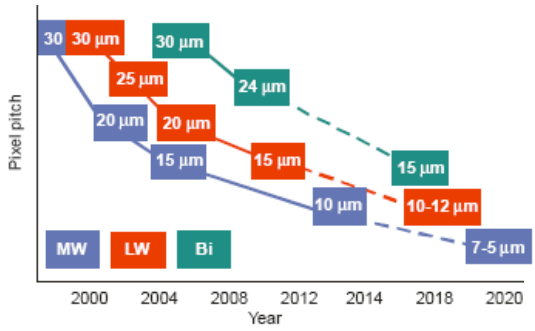

Fig. 16. Pixel pitch for HgCdTe photodiodes [34].

Concerning the system based on QWIPs, one should point out that the state-of-the-art of QWIP and HgCdTe FPAs can provide rather similar performance for figure of merit (see Table 2), but the integration time of QWIP FPAs is from 10 to 100 times longer because of the low quantum efficiency ($\eta < 0.1$) and narrow spectral sensitivity ($\Delta\lambda/\lambda \sim 0.1$) of these detectors. The short integration time of LWIR HgCdTe devices of typically below 100 μs is useful to freeze out a scene with rapidly moving objects.

Many applications require simultaneous detection in the two IR spectral bands. Both HgCdTe and QWIP give the possibility to design at least two-color FPAs at the same substrate to fabricate them from multilayer materials. But because of narrow $\Delta\lambda/\lambda$, QWIPs can be well adjusted detectors for the fabrication of two-color IR FPAs, since QWIPs absorb IR radiation only in a narrow spectral band, and they are transparent outside of that absorption band.

3.2. Thermal detectors. Upper limit performance

Thermal detector arrays are now produced in larger volumes as compared to all other IR arrays together [6]. Performance of microbolometer arrays now achieved in 8–14 μm spectral range is approaching to the theoretical physical limits, though they are worse as compared to cooled FPAs, but have the advantages in weight, power consumption, and cost. To a great degree, the uncooled sensor systems enable the creation of new means not driving closer to "physical limits" but by tailoring designs and performance to be well matched to the specific applications, e.g. for "staring" thermovision devices in civilian and military systems.

Initially developed for the military market by US defence companies ("military uncooled camera markets are mainly driven by the huge US Military demand: more than 85% of the world market" [35]), IR uncooled cameras are now widely used in many commercial applications (surveillance, commercial vision, etc.). Currently, the microbolometer detectors are produced in larger volumes than all other IR array technologies together. Their predicted cost seems should be dropped. It is expected that commercial applications in surveillance, automotive and thermography will reach total volumes more than 1.1 million units in 2016 ($3.4 B in value) (see Fig. 17).

In the IR there remains a steady emphasis on improving uncooled microbolometers that will continue to mature with smaller detector sizes and larger formats. Current products utilize the 17 μm pitch and are available in high-definition formats (640 and 1280) primarily in the LWIR band (though for most of them not available outside the producer countries). MWIR arrays have also been fabricated, but they are limited by detector noise (see Table 3 below). In the near future, uncooled 10–12 μm detector pitch arrays seems to be available in high-definition format (1920×1080). This reduction in pitch will enable a reduction in optics size

© 2012, V. Lashkaryov Institute of Semiconductor Physics, National Academy of Sciences of Ukraine

allowing increased range capability without any increase in weight for man-portable applications.

Microbolometer sensor technologies are the dominant IR thermal uncooled detector technologies whose cost is dropping down quickly. Perhaps, it can be assumed that VO_x, which now is the dominant microbolometer material (see Fig. 7), will be replaced by silicon based material (e.g., α-Si) thanks to their promising cost and manufacturability preferences in silicon foundries, though from the point of view of [12] VO_x detectors can also be produced in silicon foundries.

The IR wavelength thermal uncooled detectors because of technological problems of manufacturing have not yet reached fundamental quantum limit characteristics, and it seems that sufficient efforts should be applied in improving the microbolometer process capability concerning, e.g., the design rules. They are not limited by background flux fluctuations noise except operation at some selected long wavelengths in the sub-Kelvin temperature region at low backgrounds [36].

The noise equivalent power (NEP) is one of the figures of merit for thermal detectors and characterizes their sensitivity. Intrinsic temperature fluctuation noise of thermal detector defines its upper NEP limit as

$$\mathrm{NEP} = \left(4k_{\mathrm{B}}T^2 G_{\mathrm{th}}\right)^{1/2}, \qquad (8)$$

where k_B is the Boltzmann constant, T – temperature of the sensitive layer, and G_{th} – thermal conductance between the detector and the heat sink. For the lower G_{th}, the lower values of NEP can be achieved. For $T \approx$ 50 mK and low thermal (phonon) conductance $G_{th} \approx$ 10 fW/K, the values of NEP $\approx 4\cdot10^{-20}$ W/Hz$^{1/2}$ can be achieved at low background fluctuations conditions (e.g. cosmic background). But for room-temperature typical VO_x or α-Si microbolometers, $G_{th} \sim 10^{-7}$ W/K and thus NEP is more than seven orders worse. For these uncooled microbolometers with dimensions ~50×50×0.5 μm, the heat capacity $C_{th} \sim 2\cdot10^{-9}$ J/K and than the thermal response time $\tau_{th} = C_{th}/G_{th} \sim 20$ ms.

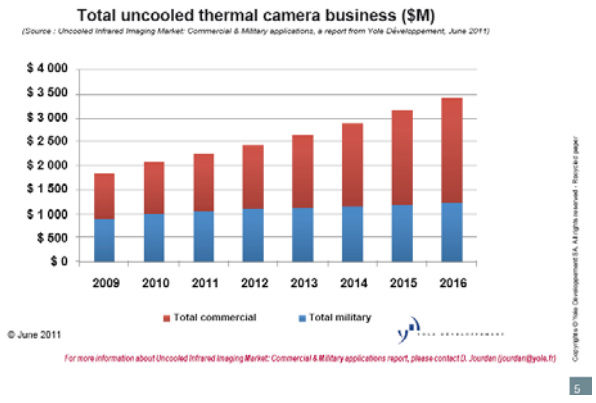

Fig. 17. Commercial and military markets predictions [35].

For ideal thermal detector being in equilibrium with an environment and with account of only temperature fluctuation noise, the typical parameters are defined by (see [6, 8, 17])

$$\mathrm{NEP} = \left(\frac{16\,\sigma_{\mathrm{B}}k_{\mathrm{B}}T^5}{\varepsilon}\right)^{1/2}\cdot\sqrt{A_d}\cdot\sqrt{\Delta f}\,, \qquad (9)$$

and detectivity is

$$D^* = \frac{\sqrt{A_d\cdot\Delta f}}{\mathrm{NEP}} = \left(\frac{\varepsilon}{16\,\sigma_{\mathrm{B}}k_{\mathrm{B}}T^5}\right)^{1/2}, \qquad (10)$$

where ε is the emissivity of detector. Than, for ε = 1 it follows for any ideal thermal detector the detectivity is wavelength independent and is not dependent on the detector area A_d, and bandwidth Δf, $D^* = 1.813\cdot10^{10}$ cm·Hz$^{1/2}$/W. For the noise equivalent power, it follows that NEP = $5.55\cdot10^{-11}(A_d\cdot\Delta f)^{1/2}$ and NEP depends on detector area and bandwidth. The thermal conductance coefficient at radiation interchange of thermal detector with the area A_d = 50×50 μm and environment at 300 K is $G_{\mathrm{rad}} = 4\varepsilon\sigma_{\mathrm{B}}T^3A_d = 1.53\cdot10^{-8}$ W/K. This thermal conductance coefficient defines the lowest possible values of G_{th}. Here, $\sigma_B = 5.67\cdot10^{-8}\,\mathrm{W\cdot m^{-2}\cdot K^{-4}}$ is the Stefan-Boltzmann constant.

For the case of temperature fluctuation noise and background fluctuation noise limited NETD, one can obtain the next expression [6, 8, 17]

$$\mathrm{NETD} = \frac{8(\mathrm{F/\#})^2\cdot\left[2k_{\mathrm{B}}\cdot\sigma_{\mathrm{B}}\cdot\left(\mathrm{T_d^5}+\mathrm{T_b^5}\right)\cdot\Delta\mathrm{f}\right]^{1/2}}{\left(\varepsilon\mathrm{A_d}\right)^{1/2}\cdot\tau_{\mathrm{op}}\cdot\int_{\lambda_1}^{\lambda_2}\frac{\partial\mathrm{W}(\lambda,\mathrm{T})}{\partial\mathrm{T}}\cdot\mathrm{d}\lambda}, \qquad (11)$$

where ε is the emissivity of detector (instead of quantum efficiency η for photon detectors), σ_B – Stefan-Boltzmann constant, k_B – Boltzmann constant, T_b – background temperature, T_d – detector temperature.

From (11), one can estimate the NETD upper limit (ideal detector). For detector with A_d = 25×25 μm, $T_d = T_b$ = 300 K, ε, τ_f, τ_{op}, τ_{atm} = 1, $\Delta f = 1/(2\tau_d)$ Hz ($\tau_d \approx \tau_{acc} \approx \tau_{th} \approx$ 20 ms), F/# = 1 in spectral range 8–14 μm NETD = 1.68 mK. Here, τ_d is the dwell time of the system, and it is accepted that for ideal thermal detector $D^* = 1.813\cdot10^{10}$ cm·Hz$^{1/2}$/W. For 3–5 μm region, it is much higher, because of $\partial W/\partial T(\lambda)$ dependence (see Fig. 11).

NETD limited values for some ideal detectors are shown in Table 3 for $T_d = T_b$ = 300 K, ε, τ_f, τ_{op}, τ_{atm} = 1, $\Delta f = 1/(2\tau_d)$ Hz ($\tau_d \approx \tau_{acc} \approx \tau_{th} \approx$ 20 ms), F/# = 1.

Taking ε, τ_f, τ_{op}, $\tau_{atm} < 1$ (e.g. taking them ~0.9) will degrade the system parameters by ~35%. For real detectors other types of noises (see Eq. (4)) can degrade the NETD parameter to several tenths of mK (see Table 4 below) and theoretical limit for 28×28 μm pixel can be NETD ≈ 12 mK [16, 25].

© 2012, V. Lashkaryov Institute of Semiconductor Physics, National Academy of Sciences of Ukraine

Table 3. NETD for ideal thermal detectors (background fluctuation noise limited) [8].

Spectral region μm	$\int(\partial W/\partial T)\cdot d\lambda$, W/(cm^2·K)	NETD, mK (A_d = 50×50 μm)	NETD, mK (A_d = 25×25 μm)
8 – 14	$2.63\cdot10^{-4}$	0.84	1.68
3 – 5	$2.13\cdot10^{-5}$	10.36	20.72
1 – 100	$6.11\cdot10^{-4}$	0.36	0.72

Some parameters of microbolometer FPAs from several manufactures are summarized in Table 4. They are typical for other cooled FPAs and are taken from [6, 8] and respective some Companies data sheets.

A comprehensive calculational model for the noise equivalent temperature difference (NETD) of infrared imaging systems based on uncooled bolometer arrays shows that the NETD model for evaluation of a possible system and bolometer design improvements allows to reach the potential value of NETD ≈ 12 mK for uncooled bolometer arrays with a bolometer pixel pitch of 28×28 μm [16, 25]. To get such microbolometer array NETD in Exp. (4), the constituents of noise are: $(\mathrm{NETD}_{1/f})^2 = (5.4\ \mathrm{mK})^2$, $(\mathrm{NETD}_{\mathrm{J-N}})^2 = (5.6\ \mathrm{mK})^2$, $(\mathrm{NETD}_{\mathrm{thermal}})^2 = (6.8\ \mathrm{mK})^2$, and $(\mathrm{NETD}_{\mathrm{ROIC}})^2 = (6.4\ \mathrm{mK})^2$. In this case, the resulting NETD would be limited mainly by the thermal fluctuation noise $\mathrm{NETD}_{\mathrm{thermal}}$ and thus, by the thermal conductance between the bolometer and its surrounding.

Microbolometer arrays are now produced in larger volumes compared to all other IR arrays together. One of the drawbacks of thermal detectors is there response time that in the case of "staring" thermovision is inessential, particularly in the case of civil applications where, as it seems, they turn the tables. But it concerns only "staring" thermovision. A lot of other applications require high operation speed and sensitivity response, which are distinctive features of quantum detectors.

If the thermal (Johnson-Nyquist) and 1/*f* noises in VO_x detectors are prevailing over other noises (as a rule) than for NETD Figure of Merit (FOM) equation [37] can be written

$$\mathrm{FOM} = \mathrm{NETD}\times\tau_{\mathrm{th}}, \qquad (12)$$

the illustration of which is depicted in Fig. 18.

The thermal noise contribution is inversely proportional to the bias voltage. Both ROIC noise and thermal noise approach the thermal fluctuation noise at rather high biases, and thermal fluctuation noise is dominated by thermal conductance of the detector legs, which can be as low as $3.5\cdot10^{-8}$ W/K [37].

Table 4. Commercial and state-of-the-art uncooled IR bolometer arrays of some manufactures for spectral band λ ≈ 8-14 μm.

Manufacturer	Material	Format	Pitch, μm	NETD, mK; optics F/1; frame rate *f* = 20-60 Hz
DRS Technologies (USA)	VO_x	320×240	17	<40
		640×480	25.4	<50
		640×480	17	<50
L-3 Communications	α-Si	320×240	30	<50
		640×480	17	<50
FLIR (USA)	VO_x	640×480	25	35
		640×512	17	<50
		320×240	37.5	50
	α-Si	640×480	30	50
ULIS (France)	α-Si	384×288	17	40
		640×480	25	<60
		640×480	17	<75
		640×480	17 (3-14 μm)	<50
		1024×768	17	<60
RAYTHEON (USA)	VO_x	320×240	50	20-35
	VO_x	320×240, 640×480	25	<50
			25	<50
	VO_x	1024×768	17	R&D
		2048×1536	17	R&D
BAE Systems (USA)	VO_x	320×240	28	30
	VO_x	640×480	28, 17	30-50
	VO_x	1024×1024	17	50
	VO_x	640×512	25	40-70
SCD (Israel)	VO_x	384×288	25	<50
		640×480	25	<50
		640×480	17	<50
NEC (Japan)	VO_x	320×240, 640×480	23.5	<75

© 2012, V. Lashkaryov Institute of Semiconductor Physics, National Academy of Sciences of Ukraine

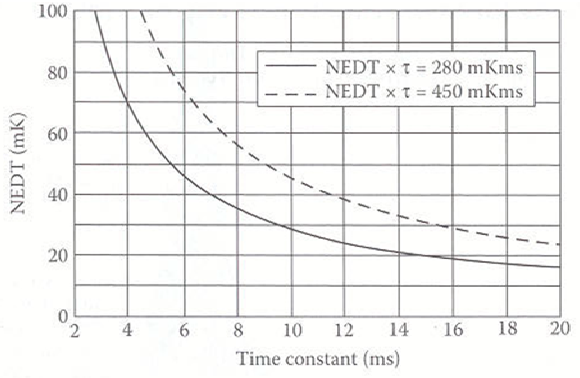

Fig. 18. Calculated microbolometer NETD and thermal time constant τ_{th} for two NETD×τ_{th} products [37].

From Fig. 18, one can see that for VO_x microbolometer arrays NETD values can reach NETD ≈ 20 mK at response times τ_{th} ~ 20 ms. In 320×240 array with 50×50 μm VO_x pixels the average NETD = 8.6 mK was achieved [38] with optics F/1.

For vision systems with rather sensitive arrays, the detection range is limited not only by pixel sensitivity but to a considerable degree, by pixel resolution. The detection range of many uncooled IR imaging systems is limited by pixel resolution rather than sensitivity. For 320×240 array (with 50×50 μm pixels) and F/1 optics with the focal length f ~ 10 cm, the minimal object size seen by one pixel at the distance 1 km will be about 0.5 m (IFOV ~ 0.5 mrad). With Thermal-Eye 250D camera (NETD ≈ 50 mK) one can detect/recognize the human being at ~ 500/300 m (objective with f = 50 mm, FOV ≈ 18°×14°) and ~ 1500/900 m (optics f = 150 mm, FOV = 6°×4.4°). The identification length will be ~2 times shorter than the recognition length. With smaller optics, these distances will be shorter. For the same optics but for the system with 640×480 array with 25×25 μm, image quality is four times better and the minimal object size is ~0.25 m.

E.g., for MCT 3–5 μm cooled array with the same number of pixels (640×480) and F/2 320 mm optics (IFOV = 0.05 mrad, pixel pitch 15 μm, FLIR MCT 1500/3000 modules) detection/recognition/identification distances are 10.5/3.2/1.7 km, respectively. Here, IFOV is instantaneous FOV.

The cost of optics that is made now from Ge and which, to a great degree, defines the cost of systems with uncooled arrays depends approximately on the square of the lenses diameter. Reducing the pixel size, one diminishes the system cost, their size and weight especially of man-portable systems (though the cost of arrays is growing, see Table 5). But reducing the pixel size, one increases the NETD (see Eq. (12)). Raytheon has started work on the HD LWIR program, which is laying the foundation for the next generation of uncooled detectors by further shrinking the pixel to <17 μm [39], that for optics F/# = F/1 is even lower than the diffraction limit in the spectral range 8–14 μm.

Table 5. Approximate costs of commercial uncooled arrays for thermal imagers [6].

Uncooled arrays	Cost, $ US
640×480 pixel, 25×25 μm bolometer arrays	15,000
384×288 pixel, 35×35 μm or 25×25 μm bolometer arrays	4000-5500
320×240 pixel, 50×50 μm bolometer arrays	3500-5000
320×240 pixel, 50×50 μm bolometer arrays for imaging radiometers*	15,000-30,000
120×1 pixel, 50×50 μm thermoelectric arrays for imaging radiometers*	<8000
320×240 pixel, 50×50 μm hybrid ferroelectric bolometer arrays imagers for driver's vision enhancement	1500-3000
160×120 pixel, 50×50 μm bolometer arrays for thermal imagers	<2000
160×120 pixel, 50×50 μm bolometer arrays for driver's vision enhancement systems	<2000
160×120 pixel, 50×50 μm bolometer arrays for imaging radiometers*	<4000

*The cost of arrays for radiometers is considerably higher and depends on specific performance requirements. Estimations given in table should be treated as approximate.

Now the thermal sensitive arrays with 17×17 μm pixel sizes are commercially available, both being manufactured on the base of VO_x and α-Si (see Table 4).

The development of sensitive 17 μm and even 12 μm pitch microbolometer arrays however presents significant challenges in both fabrication improvements and pixel design connected with performance degradation as the unit cell is reducing. "This problem can be mitigated to some degree, if the microbolometer process capability (design rules) is improved dramatically" [6].

Conventional single-level bolometer arrays typically have the fill factor of 60 to 70% [40, 41]. To increase the fill factor, two-layer bolometer design was developed allowing to get it up to 90% [42, 43].

Two-layer "umbrella design" let to get 17×17 μm pixel size [40]. The bolometer legs, and in some cases the sensing material, are placed underneath the bolometer absorbing layer. In another two-layer 17×17 μm pixel size design (double-layer micromachining process), the thermal isolation layer is fabricated on the first level and the optical absorber level is produced on the second level of the structure [44].

4. Thermal detectors vs. photon detectors

One of the main differences in thermal un-cooled and photon detectors is that thermal detectors mainly depend upon macroscopic material properties, whereas photon detectors depend upon microscopic features. Thermal

© 2012, V. Lashkaryov Institute of Semiconductor Physics, National Academy of Sciences of Ukraine

detector has their own advantages, the principle one being the relative crudeness of the detector material requirements. And this is one of outcomes of the cost of arrays production [45] but not for the systems on their base, e.g. radiometers, in which the cost is mainly governed by specific performance requirements and it can be relatively high.

An analysis of operation of photon and uncooled thermal detectors comparing $NETD_{th}/NETD_{ph}$ via expressions (3) and (11) shows that only the background fluctuation noise limits performance of thermal detectors in 8–14 μm region (without account of other noises in Eq. (4)). For the same other parameters, it is ≈4.6 times worse than that of photon detectors (under BLIP conditions at $T_d \approx T_b \approx 300$ K). If one takes the spectral band 8–12 μm for photon detectors and 8–14 μm for thermal detectors, this ratio will be ≈4.1. When comparing the data of Tables 2 and 4, one can see that the ratio $NETD_{th}/NETD_{ph}$ is not so noticeable for 8–14 μm region, but one should take into consideration that the NETD data for photon arrays were obtained as a rule with optics F/# ≥ F/2 (smaller input diameter and thus cheaper-to-make) which degrades the NETD parameter as $(F/\#)^2$.

For 3–5 μm region, the difference is much more distinct (≈15 times worse for thermal detectors) and much higher for 1–2.5 μm spectral range.

As a rule, photon detectors are now operating in BLIP regime, whereas thermal detectors have not yet reach the BLIP regime up to date, and it seems no one really knows how to get a BLIP-limited small pixel thermal detector arrays regime.

Because of it, thermal detectors are not effective detectors for 3–5 or 1–2.5 μm spectral regions. The basic reason for that is the steepness of function $\frac{\partial W(\lambda,\dot{O})}{\partial T}$ in the denominators of (3) and (11) quickly declining in shorter, compared to $\lambda \approx 8$ μm, wavelengths. In photon detectors, this $\frac{\partial W(\lambda,\dot{O})}{\partial T}$ falling is compensated, to a great extent, by growing D^*_λ with λ_{co} decrease. In thermal detectors, D^* does not depend on the wavelength. This situation discriminates photon detectors from thermal ones, and thus the systems with photon detectors operating in $\lambda < 8$ μm spectral bands (3-5 and 1-2.5 μm) will have principally better parameters compared to system with thermal FPAs. This means that technical vision systems will have principally better parameters as concerning the thermal contrast, distances of acquisition and recognition, etc. However, the parameters gained by thermal detectors (microbolometers) today are sufficient for a lot of commercial and special applications needed of lightweight, low consumption power and relatively cost-effective thermal imagers. As uncooled thermal arrays operate at F/# ≈ F/1 conditions (because of internal noises (see, e.g. (4), in which, except background fluctuation noise, also Johnson-Nyquist and 1/*f* ones are important) their operation cannot be improved at smaller FOVs, as compared to cooled detectors with smaller NEPs (and smaller FOVs with cooled diaphragms), and the distances of detection and recognition for cooled photon FPAs will be larger.

Another drawback of thermal detectors and FPAs is their response time that still in the case of "staring" thermovision systems is inessential.

Photon and thermal detectors are optimally suited for different types of applications. The design and manufacturing barriers to achieve BLIP conditions for small pixel area thermal detector arrays still are challengeable. And from this viewpoint, despite serious competition from alternative technologies, MCT arrays are unlikely to be seriously challenged in the near future for high-performance applications, requiring multispectral capability and high frequency frame operation.

5. Summary

Short analysis of operation photon and thermal arrays shows that these detector arrays are suited for different types of applications. Cues to progress in developing of these devices can be obtained from knowledge of what is happening in research and development institutions, but it should be pointed out that actual system deployment requires highly developed technological processes and production capabilities which can't exist in every country. At the same time high performance IR FPAs are controlled by security classification and export restrictions.

One can conclude that HgCdTe will remain material of choice for at least the next 10–15 years, as the arrays on the base of it have near theoretical performance in several spectral bands. HgCdTe is unlikely to be seriously challenged for high-performance applications, requiring multispectral capability, long acquisition, recognition and identification distances, and also fast response.

Quick application of civilian IR technologies is mainly connected with powerful development of uncooled cameras. Currently, the microbolometer arrays are produced in larger volumes than all other IR array technologies together and it is predicted that this tendency will be increased in the future.

Still it can be concluded that the design and manufacturing barriers to achieve BLIP conditions for small pixel area thermal detector arrays are quite challengeable. Small pixels in arrays allow the implementation of high-resolution FPAs. At the same time the important reason is the cost for both the FPA chip and for the infrared optics is reduced by reducing the active area of the FPA. To date the dimensions of pixels and NETD values in conventional and under R&D IR photon arrays are smaller compared to those ones in thermal FPAs resulting in better resolution and longer distances of detection, recognition and identification (in the systems with the same optics).

© 2012, V. Lashkaryov Institute of Semiconductor Physics, National Academy of Sciences of Ukraine

Though the sensitivity, pixel sizes and their number of microbolometer arrays are not as good as the cooled photon ones, however they are sufficient for a lot of commercial and special applications needed of lightweight, low consumption power and relatively cost-effective thermal imagers.

One of the drawbacks of thermal detectors is their response time that in the case of "staring" thermovision systems is inessential particularly in the case of civil applications where, as it seems, they turn the tables. But it concerns only "staring" thermovision. A lot of other applications require high operation speed and sensitivity which are distinctive features of photon detector arrays. Moreover in many applications there exist the needs of multicolor thermovision for which thermal detectors are much less applicable because of fast NETD increase when going to a shorter spectral band from $\lambda \sim 8$ μm, compared to photon detectors.*)

*) Note added in Proofs.

Initially developed for the military market by US defense companies, IR uncooled technologies are now widely used in many commercial applications. While the number of infrared systems shipped into the military market over that period is predicted to decline, the commercial market for such systems would appear to be growing significantly [46]. According to the Yole Developpement latest report "Uncooled Infrared Imaging: Commercial & Military Applications" (Yole Développement (Lyon-Villeurbanne, France)), sales of uncooled IR cameras will grow from 320,000 units in 2011 to 1.1 million units in 2017. The market share for uncooled IR imagers for commercial applications will represent more than 80 per cent of the total uncooled IR imaging market, with the slice for military applications shrinking from around 30 to 15 per cent.

References

1. *Seeing Photons: Progress and Limits of Visible and Infared Sensor Arrays*, Committee on Developments in Detector Technologies; National Research Council, ISBN 978-0-309-15304-1 (2010).
2. E.S. Barr, Historical survey of the early development of the infrared spectral region // *Amer. J. Phys.* **28**, p. 42-54 (1960).
3. R.A. Smith, F.E. Jones and R.P. Chasmar, *The Detection and Measurement of Infrared Radiation.* Clarendon, Oxford, 1958.
4. R.D. Hudson, *Infrared System Engineering*. Wiley-Interscience, New Jersey, 1969.
5. L.M. Biberman and R.L. Sendall, Chapter 1. Introduction: A brief history of imaging devices for night vision, in: *Electro-Optical Imaging: System Performance and Modeling*, edited by L.M. Biberman. SPIE Press, Bellingham, p. 1-1–1-26 (2000).
6. A. Rogalski, *Infrared Detectors* (2nd edition). CRC Press, Boca Raton, 2011.
7. A.S. Gilmore, High-definition infrared FPAs // *Raytheon Technology Today*, issue 1, p. 4-8 (2008).
8. F. Sizov, *Photo-electronics for Vision Systems in Invisible Spectral Ranges*. Academperiodika, Kiev, 2008 (in Russian).
9. N. Sclar, Properties of doped silicon and germanium infrared detectors // *Progr. Quantum Electron.* **9**, p. 149-257 (1984).
10. B.A. Volkov, L.I. Ryabova, and D.R. Khokhlov, Mixed-valence impurities in lead telluride-based solid solutions // *Physics-Uspekhi,* **45**, p. 819-846 (2002).
11. R.A. Wood, Uncooled microbolometer infrared sensor arrays, in: *Infrared Detectors and Emitters: Materials and Devices* / P. Capper, C.T. Elliott / p. 149-175. Kluwer Academic Publishers, Norwell, USA, 2001.
12. *Uncooled detectors for thermal imaging cameras*, FLIR Technical Note, *http://www.flir.com/uploadedFiles/Eurasia/Cores_and_Components/Technical_Notes/uncooled%20detectors%20BST.pdf.*
13. R. Hartmann, M. Selders, High-sensitivity thin-film bolometers // *Proc. Sensor 1982 – Sensor Technology and Temperature Measurement*, Essen, p. 102-116 (1982).
14. K.C. Liddiard, Thin-film resistance bolometer IR detectors // *Infr. Phys.,* **24**, p. 57-64 (1984).
15. R.A. Wood, J. Carney, R.E. Higashi, T. Ohnstein, J. Holmen, Advances in un-cooled silicon monolithic IR 2D arrays // *Proc. IRIS DSG*, 1988.
16. F. Niklaus, C. Vieider, MEMS-Based uncooled infrared bolometer arrays – a review // *Proc. SPIE,* **6836**, p. 68360D (2007).
17. P. Kruse, *Uncooled Thermal Imaging. Arrays, Systems, and Applications*. SPIE Press, Bellingham, USA (2001).
18. A.M. Filachev, V.P. Ponomarenko, I.I. Taubkin, M.B. Ushakova, Infrared focal plane arrays: state of the art and development trends // *Proc. SPIE*, **5126**, p. 52-85 (2003).
19. S. Horn, D. Lohrmann, J. Campbell, P. Perconti, and R. Balcerack, Uncooled IR technology and applications // *Proc. SPIE*, **4369**, p. 210-221 (2001).
20. A. Hoffman, Semiconductor processing technology improves resolution of infrared arrays // *Laser Focus World*, 81–84, February (2006).
21. A.H. Lettington, I.M. Blankson, M. Attia, and D. Dunn, Review of imaging architecture // *Proc. SPIE,* **4719**, p. 327-340 (2002).
22. I.I. Taubkin and M.A. Trishenkov, Infromation capacity of electronic vision systems // *Infrared Phys. Technol.*, **37**, p. 675-693 (1996).
23. T. Sprafke, and J.W. Beletic, High performance IR focal plane arrays // *Optics & Photonics News*, **19**, p. 22-27 (2008).

© 2012, V. Lashkaryov Institute of Semiconductor Physics, National Academy of Sciences of Ukraine

24. G.C. Holst, *Electro-Optical Imaging System Performance*. SPIE Opt. Eng. Press, Bellingham, 2003.
25. F. Niklaus, A. Decharat, C. Jansson, G. Stemme, Performance model for uncooled infrared bolometer arrays and performance predictions of bolometers operating at atmospheric pressure // *Infrared Phys. Technol.*, **51**, p. 168-177 (2008).
26. V.V. Vasil'ev, A.V. Predein, V.S. Varavin, N.N. Mikhailov, S.A. Dvoretskii, V.P. Reva, I.V. Sabinina, Yu.G. Sidorov, A.O. Suslyakov, A.L. Aseev, and F.F. Sizov, Linear 288×4-format photodetector with a bidirectional time-delay-and-storage regime // *J. Opt. Techn*., **76**, p. 757-761 (2009).
27. A.I. D'Souza, L.C. Dawson, D.J. Berger, S. Clark, P.S. Wijewarnasuriya, J. Bajaj, J.M. Arias, W.E. Tennant, L. Kozlowski, K. Vural, HgCdTe detectors and FPAs for remote sensing applications // *Proc. SPIE*, **3698**, p. 538-544 (1999).
28. P. Tribolet, P. Chorier, A. Manissadjian, P. Costa, and J.-P. Chatard, High performance infrared detectors at Sofradir // *Proc. SPIE*, **4028**, p. 438-456 (2000).
29. L.J. Kozlowski, K. Vural, J.M. Arias, W.E. Tennant, and R.E. DeWames, Performance of HgCdTe, InGaAs and quantum well GaAs/AlGaAs staring infrared focal plane arrays // *Proc. SPIE*, **3182**, p. 2-13 (1997).
30. H.M. Runciman, Influence of technology on FLIR waveband selection // *Proc. SPIE*, **2470**, p. 156-166 (1995).
31. L. Kozlowski, HgCdTe focal plane arrays for high performance infrared cameras // *Proc. SPIE*, 3179, p. 200-211 (1997).
32. I.I. Taubkin, M.A. Trishenkov, and N.V. Vasilchenko, Minimum temperature difference detected by the thermal radiation of objects // *Infrared Phys. Technol.*, **35**, p. 715-732 (1994).
33. P. Norton, B. Andresen, G. Fulom, Introduction // *Proc. SPIE*, **6940**, p. XIX-XXXVI (2008).
34. G. Destefanis, P. Tribolet, M. Vuillermet, and D.B. Lanfrey, MCT IR detectors in France // *Proc. SPIE,* **8012**, 801235-1–12 (2011).
35. A.M. Fitzgerald, Uncooled IP market will boom // *Micronews*, Issue #114, p. 3-5 (2011).
36. A. Rogalski, F. Sizov, Terahertz detectors and focal plane arrays // *Optoelectron. Rev*., **19**, p. 346-404 (2011).
37. M. Kohin, and N. Butler, Performance limits of uncooled VO_x microbolometer focal-plane arrays // *Proc. SPIE*, **5406**, p. 447-453 (2004).
38. W. Radford, D. Murphy, A. Finch, K. Hay, A. Kennedy, M. Ray, A. Sayed, et al., Sensitivity improvements in uncooled microbolometer FPAs // *Proc. SPIE*, **3698**, p. 119-130 (1999).
39. S.H. Black, T. Sessler, E. Gordon, R. Kraft, T. Kocian, M. Lamb, R. Williams, and T. Yang, Uncooled detector development at Raytheon // *Proc. SPIE*, **8012**, 80121A-1–12 (2011).
40. C. Li, G.D. Skidmore, C. Howard, C.J. Han, L. Wood, D. Peysha, E. Wlliams et al., Recent development of ultra small pixel uncooled focal plane arrays at DRS // *Proc. SPIE*, **6542**, p. 65421Y (2007).
41. E. Mottin, A. Bain, J. Martin, J. Ouvrier-Buffet, S. Bisotto, J.J. Yon, and J.L. Tissot, Uncooled amorphous silicon technology enhancement for 25 μm pixel pitch achievement // *Proc. SPIE*, **4820**, p. 200-207 (2003).
42. D. Murphy, M. Ray, A. Kennedy, J. Wyles, C. Hewit, R. Wyles, E. Gordon et al., High sensitivity 640×512 (20 μm pitch) microbolometer FPAs // *Proc. SPIE*, **6206**, p. 62061A (2006).
43. S. Tohyama, M. Miyoshi, S. Kurashina, N. Ito, T. Sasaki, A. Ajisawa, and N. Oda, New thermally isolated pixel structure for high-resolution uncooled infrared FPAs // *Proc. SPIE*, **5406**, p. 428-436 (2004).
44. S. Black, M. Ray, C. Hewitt, R. Wyles, E. Gordon, K. Almada, S. Baur, M. Kuiken, D. Chi, and T. Sessler, RVS uncooled sensor development for tactical applications //*Proc. SPIE*, **6940**, p. 694022 (2008).
45. Ch.M. Hanson, Uncooled IR detector performance limits and barriers // *Proc. SPIE*, **4028**, p. 2-11 (2000).
46. D. Wilson, Report focuses in on the infrared market, *Vision System Design*, June, 15 (2012).

© 2012, V. Lashkaryov Institute of Semiconductor Physics, National Academy of Sciences of Ukraine